Composite Structures 160 (2017) 36–42

Contents lists available at ScienceDirect

Composite Structures

journal homepage: www.elsevier.com/locate/compstruct

Crack swarm inspection for estimation of crack location in carbon fiber reinforced plastics: A numerical study

Ryosuke Matsuzaki [a,*], Kentaro Yamamoto [a], Akira Todoroki [b]

[a] Department of Mechanical Engineering, Tokyo University of Science, 2641 Yamazaki, Noda, Chiba 278-8510, Japan
[b] Department of Mechanical Sciences and Engineering, Tokyo Institute of Technology, 2-12-1 Ookayama, Meguro, Tokyo 152-8552, Japan

ARTICLE INFO

Article history:
Received 22 May 2016
Revised 7 October 2016
Accepted 8 October 2016
Available online 11 October 2016

Keywords:
Laminate
Delamination
Electrical properties
Anisotropy
Non-destructive testing

ABSTRACT

The present study proposes crack swarm inspection (CSI) for estimating crack location and size in carbon composite laminates from the surface voltage distribution. This technique generates a large number of virtual microscopic cracks, and calculates the surface voltage distribution of the composites using anisotropic electric potential functions and doublet strings. Using genetic algorithms, the virtual microscopic cracks formed a swarm to coincide with the measured surface voltage; thereby, the crack sizes and locations are estimated from the position of the crack swarm. The CSI was applied to crack detection in carbon laminated composite plates; it was confirmed that the existence of cracks in each partitioned section was detected with >80% probability, in reference to the crack location and size information. Furthermore, we also confirmed that the estimation accuracy was affected by the electric current density in the thickness direction, and addressed the recommended electrode interval based on the minimum size of the estimated crack.

1. Introduction

The applications of carbon fiber reinforced plastics (CFRPs) have expanded, particularly in the field of aeronautics, because of its outstanding specific strength and stiffness as compared with metals [1,2]. However, when CFRP laminated plates are used as a structural component, even small impacts can easily lead to delamination, considerably reducing strength [3]. To ensure the structural integrity (and to reduce the high costs incurred by periodic inspections), there is an urgent need for a health monitoring system for CFRP laminated plates. Previously, the following nondestructive inspection techniques have been used: ultrasonic inspection [4–6], X-ray inspection [7,8], acoustic emission (AE) [9,10], optical fiber inspection [11–13], and visual inspection. However, these methods are costly and time-consuming, or may decrease the structural strength by requiring an embedded sensor. Against this backdrop, there is a demand for a simple, non-destructive health monitoring process that detects delamination during periodic inspections or during operation. The monitoring method must be suitable for existing structures, and must not cause a reduction in strength by requiring sensors to be embedded.

As a useful health monitoring technique that can be applied during operation, the electrical resistance change method [14,15] has been proposed for monitoring fiber fractures [16,17], strain [18], and fatigue [19]. In this technique, the electrical resistances that arise because of delamination are measured using electrodes attached to the structural surface, so as not to cause a reduction in strength. The suggested technique was applied to monitoring the occurrence of delamination in CFRP laminated plates based on changes in the electrical resistance between a number of electrodes on the CFRP surface [20–23]. However, this method does present complex challenges for measurement systems because it is necessary to measure the electrical resistance of every current in all of the spaces between adjacent electrodes to measure the delamination-dependent changes in electrical resistance between electrodes. To address this problem, the electric potential difference technique is used; it involves installing a pair of electric current electrodes and a large number of voltage electrodes, making it possible to identify cracks using a single electric current [24–27]. However, these techniques require multiple tests and expensive numerical analyses; thus, there is a need to develop a technique that is simpler to implement.

A simple technique has been proposed for analyzing electric current density in CFRP, in which changes in voltage due to delamination are analyzed by installing a string of anisotropic doublets at separation points [28,29]. This technique makes it possible to

* Corresponding author.
E-mail address: rmatsuza@rs.tus.ac.jp (R. Matsuzaki).

http://dx.doi.org/10.1016/j.compstruct.2016.10.020
0263-8223/

analyze the electric current density of a CFRP laminated plate using a mirror image relationship. However, even though it is possible to calculate voltage changes with this technique in situations where delamination is known to have occurred, it is difficult to estimate the location and size of delamination from the voltage change.

Therefore, in this research, crack swarm inspection (CSI) is proposed, which estimates crack size and location based on a large number of virtual microscopic cracks in the inner layers of the CFRP using anisotropic electric potential functions and doublet strings. A genetic algorithm (GA) is used to minimize the difference with the voltage true value distribution and voltage distribution with virtual microscopic cracks in CFRP by changing the virtual crack position; thereby, the virtual cracks form a swarm, and the crack location and size are estimated from the crack swarm. CSI is applied to crack detection in unidirectional laminated plates, and its validity is investigated.

2. Crack estimation with crack swarm inspection

2.1. Overview of CSI

Fig. 1(a) shows a schematic diagram of the CSI method. CSI is a technique for estimating cracks by simulating many virtual cracks, which approximate the voltage distribution of damaged CFRP. One benefit is that this method allows estimation of internal cracks using only the surface voltage distribution data. The analysis process involves calculating the electric current density distribution in CFRP using an anisotropic potential function, and producing a large number of virtual microscopic cracks (unit cracks) by installing doublets [30] to oppose the electric current density in the thickness direction at the crack locations. This technique allows the position and size of cracks to be estimated using a genetic algorithm, which treats the position of cracks as a design variable, to minimize the difference between the surface voltage distribution of a CFRP that has crack swarm, and the real-world value of the voltage distribution measured in a cracked CFRP. This approach is shown in Fig. 1(b). In the present study, the aim is to investigate the delaminations in a unidirectional CFRP; as such, the virtual cracks modeled by doublets are placed in parallel to the specimen surface. To extend this to the estimation of transverse cracks in the multidirectional laminates, the directions of the doublets should be arbitrary and treated as variables.

2.2. Analysis of electrical current density using anisotropic electrical potential function

The electric potential function ϕ is calculated using the Cartesian coordinate system: the direction that the fibers are arranged into is labeled x, the transverse direction is labeled y, the thickness direction is labeled z; the current densities i_x, i_y, i_z are calculated using the following equations [31].

$$\begin{aligned} i_x &= -\sigma_x \frac{\partial \phi}{\partial x} \\ i_y &= -\sigma_y \frac{\partial \phi}{\partial y} \\ i_z &= -\sigma_z \frac{\partial \phi}{\partial z} \end{aligned} \tag{1}$$

Here, σ_x, σ_y, σ_z refer to the electric conductivity of the CFRP in the direction of the fiber, the transverse direction, and the thickness direction, respectively. If there is no electrical current source, the following equation can be derived from the equation of continuity.

$$\frac{\partial}{\partial x} i_x + \frac{\partial}{\partial y} i_y + \frac{\partial}{\partial z} i_z = 0 \tag{2}$$

If σ_x, σ_y, σ_z are constant regardless of location, then the following equation can be derived by substituting equation (2) into Eq. (1).

$$\sigma_x \frac{\partial^2 \phi}{\partial x^2} + \sigma_y \frac{\partial^2 \phi}{\partial y^2} + \sigma_z \frac{\partial^2 \phi}{\partial z^2} = 0 \tag{3}$$

Here, two dimensions, the fiber direction and the thickness direction, are considered. When a coordinate axis affine transformation is carried out as in Eq. (4), the Laplace equation shown in Eq. (5) is obtained.

$$\xi = \frac{x}{\sqrt{\sigma_x}}, \quad \eta = \frac{z}{\sqrt{\sigma_z}} \tag{4}$$

$$\frac{\partial^2 \phi}{\partial \xi^2} + \frac{\partial^2 \phi}{\partial \eta^2} = 0 \tag{5}$$

Eq. (5) resembles the velocity potential of an irrotational ideal fluid. Fig. 2(a) shows a schematic drawing of a CFRP beam with thickness t, which is the object of the anisotropic electric potential function. If there are current and earth electrodes on the same side of the CFRP beam, the electric current density analysis can be carried out on the CFRP using the velocity potential of an ideal fluid by setting the current electrode as a source point and the earth electrodes as a sink point. Assuming that the source (electric current load point) coordinates are $(-a, 0)$, and the sink (ground point) coordinates are $(a, 0)$ where $a > 0$, the electric current density is given by [28]

$$\begin{aligned} i_x &= \frac{I}{\pi\sqrt{\sigma_x \sigma_z}} \left\{ \frac{x+a}{\frac{(x+a)^2}{\sigma_x} + \frac{z^2}{\sigma_z}} - \frac{x-a}{\frac{(x-a)^2}{\sigma_x} + \frac{z^2}{\sigma_z}} \right\} \\ i_z &= \frac{I}{\pi\sqrt{\sigma_x \sigma_z}} \left\{ \frac{z}{\frac{(x+a)^2}{\sigma_x} + \frac{z^2}{\sigma_z}} - \frac{z}{\frac{(x-a)^2}{\sigma_x} + \frac{z^2}{\sigma_z}} \right\} \end{aligned} \tag{6}$$

Furthermore, when analyzing thin laminates, an affine-transformed ξ-η coordinate system contains an isotropic space; therefore, it is

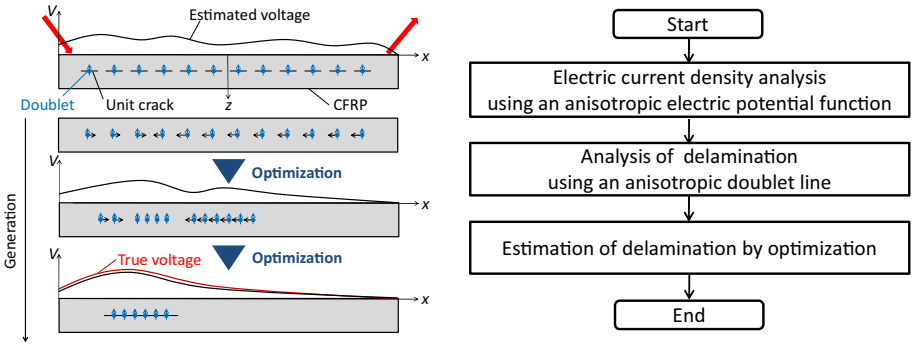

Fig. 1. Schematic of crack swarm inspection. (a) Basic concept for detection of cracks inside CFRP. (b) Flowchart of CSI.

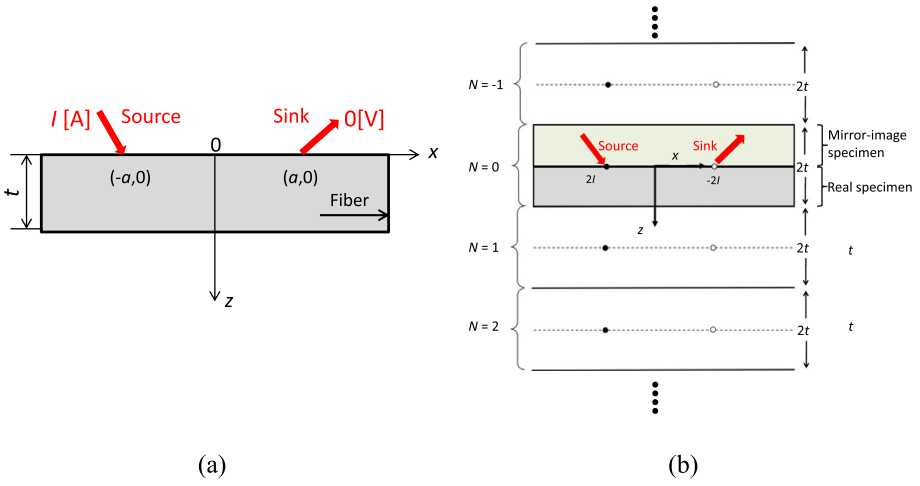

Fig. 2. Schematic of anisotropic electric potential function. (a) Specimen configuration. (b) Image method for electric current in a thin CFRP laminate.

possible to simulate the current density in the thickness direction by installing a number of mirror images in the same way as the velocity potential of an ideal fluid [29]. Here, taking N as the set of positive and negative mirror images, if the mirror images are drawn as shown in Fig. 2(b), the current density for the $N = n$ set is derived as shown below, by summing from $N = -n$ to $N = n$.

$$i_x = \sum_{k=-n}^{n} \frac{I}{\pi\sqrt{\sigma_x\sigma_z}} \left\{ \frac{x+a}{\frac{(x+a)^2}{\sigma_x}+\frac{(z-2tk)^2}{\sigma_z}} - \frac{x-a}{\frac{(x-a)^2}{\sigma_x}+\frac{(z-2tk)^2}{\sigma_z}} \right\}$$
$$i_z = \sum_{k=-n}^{n} \frac{I}{\pi\sqrt{\sigma_x\sigma_z}} \left\{ \frac{z-2tk}{\frac{(x+a)^2}{\sigma_x}+\frac{(z-2tk)^2}{\sigma_z}} - \frac{z-2tk}{\frac{(x-a)^2}{\sigma_x}+\frac{(z-2tk)^2}{\sigma_z}} \right\} \tag{7}$$

2.3. Delamination analysis using anisotropic doublets

The problem of delamination in a laminated plate can be modeled as a plate existing inside a fluid, because delamination cuts off the electric current at that particular location. A plate existing inside a fluid can be implemented by arranging a plate into a position that negates the vertical current. Accordingly, to create a delamination, a doublet is put in place such that it will negate the electric current density in the thickness direction at the desired position.

Consider a situation in which a crack is positioned from (x_1, z_0) on the left to (x_2, z_0) on the right; in this area the doublet's strength distribution is set at $\mu(x)$. The z coordinate starting point is translated to the position of the delamination, as z' ($z' = z - z_0$). The current density $i_{z,\,d}\,(x,\,z')$ in the thickness direction, as created by the doublet, is given by [29]

$$i_{z,d}(x,z') = -\frac{\sqrt{\sigma_z}}{2\pi}\int_{x_1}^{x_2} \mu(s) \frac{\left(\frac{x-s}{\sqrt{\sigma_x}}\right)^2 - \left(\frac{z'}{\sqrt{\sigma_z}}\right)^2}{\left\{\left(\frac{x-s}{\sqrt{\sigma_x}}\right)^2 + \left(\frac{z'}{\sqrt{\sigma_z}}\right)^2\right\}^2} ds \tag{8}$$

If the electric current density in the thickness direction as created by the anisotropic electric potential function is set as $i_z\,(x,\,z')$, then this leads to delamination by satisfying the integral equation below, which determines the doublet's strength.

$$i_z(x,0) + i_{z,d}(x,\varepsilon) = 0 \tag{9}$$

Because $i_{z,\,d}\,(x,\,0)$ is an improper integral equation, this peculiarity is eliminated by approximating $z' = \varepsilon$ (an extremely small, positive number). From the strength of the doublets referred to in Eq. (9), a voltage distribution with a crack is given by

$$V(x,z) = \phi'(x,z_0) - \phi'_0(x,z_0) = -\frac{1}{2\pi\sqrt{\sigma_x}}\int_{x_1}^{x_2} \mu(s) \frac{\frac{z_0}{\sqrt{\sigma_z}}}{\left(\frac{x-s}{\sqrt{\sigma_x}}\right)^2 + \left(\frac{z_0}{\sqrt{\sigma_z}}\right)^2} ds \tag{10}$$

where φ' and φ'_0 are the electric potential on the surface of the CFRP laminates before and after crack occurrence, respectively. Because the conductivity of CFRP in the thickness direction is miniscule compared to that in the direction of the fibers, and the electrical current flowing in the thickness direction is generally small, the mirror image is only on the upper part of $N = 0$, as shown in Fig. 2 (b). The remaining mirror images are disregarded so as to simplify calculations. According to the crack in the mirror image at $N = 0$, the surface voltage distribution created by the doublet is twice as large; thus, Eq. (10) can be transformed into the following equation.

$$V(x,z) = 2\{\phi'(x,z_0) - \phi'_0(x,z_0)\} = -\frac{1}{\pi\sqrt{\sigma_x}}\int_{x_1}^{x_2} \mu(s) \frac{\frac{z_0}{\sqrt{\sigma_z}}}{\left(\frac{x-s}{\sqrt{\sigma_x}}\right)^2 + \left(\frac{z_0}{\sqrt{\sigma_z}}\right)^2} ds \tag{11}$$

In CSI, the current electrode interval (integral interval) that constitutes the search area is divided into equal parts N_s. Within each interval N_s, the doublet strength is set at a fixed value. If a doublet is set such that the electric current density at the median x_c^k of each interval is $i_z(x_c^k, 0)$, then Eq. (9) can be written as follows.

$$i_z(x_c^k,0) - \sum_{j=1}^{N_s} \mu_j B_{kj} = 0 \tag{12}$$

$$B_{kj} = \int_{x_{j-1}}^{x_j} \frac{\sqrt{\sigma_z}}{2\pi} \frac{\left(\frac{x_c^k-s}{\sqrt{\sigma_x}}\right)^2 - \left(\frac{\varepsilon}{\sqrt{\sigma_z}}\right)^2}{\left\{\left(\frac{x_c^k-s}{\sqrt{\sigma_x}}\right)^2 + \left(\frac{\varepsilon}{\sqrt{\sigma_z}}\right)^2\right\}^2} ds \tag{13}$$

Eq. (12) can be written as the following matrix.

$$\begin{pmatrix} B_{1,1} & \cdots & B_{1,N_s} \\ \vdots & \ddots & \vdots \\ B_{N_s,1} & \cdots & B_{N_s,N_s} \end{pmatrix} \begin{pmatrix} \mu_1 \\ \mu_2 \\ \vdots \\ \mu_{n_s} \end{pmatrix} = \begin{pmatrix} i_z(x_c^1,0) \\ i_z(x_c^2,0) \\ \vdots \\ i_z(x_c^{N_s},0) \end{pmatrix} \tag{14}$$

The doublet strength of each interval μ_j ($j = 1,2,\ldots,N_s$) can be found by calculating the inverse of matrix **B**. The surface voltage is derived from Eq. (11) as follows.

$$V(x,0) = -\frac{1}{\pi\sqrt{\sigma_x}}\sum_{j=1}^{N_s}\mu_j\int_{x_{j-1}}^{x_j}\frac{\frac{z_0}{\sqrt{\sigma_z}}}{\left(\frac{x-s}{\sqrt{\sigma_x}}\right)^2+\left(\frac{z_0}{\sqrt{\sigma_z}}\right)^2}ds \quad (15)$$

2.4. Estimating crack location with optimization

The optimization method in CSI uses GA [32] for estimation of crack position and size. The optimization process is described below.

Step 1: Initial swarm creation

In CSI, a large number of unit cracks are created in the space between current electrodes. Here, to translate the condition of the unit cracks between electrodes into individuals in GA, the crack existence constant ζ is introduced. If a crack is present, then the crack existence constant is set at $\zeta = 1$, and if there is no crack present, then it is set at $\zeta = 0$. For example, the relationships between phenotype (PTYPE) and genotype (GTYPE) are shown in Fig. 3 for scenarios where a 2-mm crack is present at position $x = -2$–0 in an electrode space ($x = -3$–3 mm), and where two 1-mm cracks are present at positions $x = -2$–-1 and $x = 1$–2. The interval is split into 1-mm increments. In this way, the unit crack position is expressed as its genotype. When the current electrode space is split into N_s intervals, the crack existence constant is expressed as a vector, as in the equation below.

$$\zeta_i \in \{0,1\} \quad (i = 1,2,\ldots,N_s) \quad (16)$$

Step 2: Assessing fitness

The fitness of each individual is defined by the difference between the true voltage on the surface of the laminates, V_{true} (x, 0), and the voltage of each individual, V_{ind} (x, 0).

$$fitness = \sum_{i=1}^{n_m}\{V_{true}(x_i,0) - V_{ind}(x_i,0)\}^2 \quad (17)$$

where n_m is the number of voltage measurement points. The position and size of the crack are estimated by minimizing the fitness in Eq. (17).

Step 3: Selection

The selection method makes use of roulette selection [32]. Roulette is a selection method that allocates a higher probability of selection to individuals with a higher degree of fitness. However, with roulette selection, it remains possible that individuals with a low degree of fitness will be selected, and a possibility that individuals with the highest degree of fitness will not be selected. To prevent individuals with a high degree of fitness from being eliminated, an elite saving strategy [32] is also used, whereby individuals with the highest degree of fitness are saved and retrieved if they are not chosen as part of the selection process.

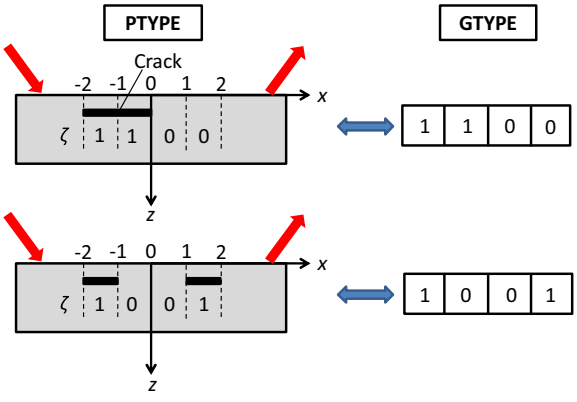

Fig. 3. Example of relationship between PTYPE and GTYPE in CSI.

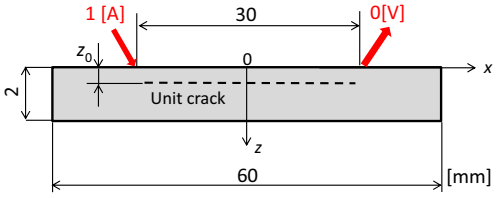

Fig. 4. Specimen configuration in CSI.

Table 1
Parameters of analytical object and conditions of each section.

Section	3.2.1	3.2.2	3.2.3
σ_z (S/m)	Variable	0.01	0.01
Number of measurement points	31	Variable	31
Depth of the crack z_0 (mm)	0.25	0.25	Variable

Step 4: Crossing and mutation

Two selected individuals are crossed, and two new individuals' genes are generated. Mutations are reflected in these two individuals' genes, and new individuals are defined. If the generation created in steps 3 and 4 satisfies the end conditions, then the process ends. If it does not satisfy the end conditions, step 2 is repeated. The end condition is a valid when the positions of unit cracks have converged.

3. CSI verification

3.1. Analytical object and conditions

A 60-mm long, 2-mm wide, 16-layer (0.125-mm thick layers) laminated plate was treated as the analytical object. As shown in Fig. 4, the origin of the x-z axis was established in the center of the test specimen, 1 A/m of current per unit width was applied at the position (x, z) = (−15, 0), and a 0-V ground voltage was established at the position (x, z) = (15, 0). The materials are modeled as a woven CFRP fabric; the conductivity is in-plane isotropic, whereas it is anisotropic in the thickness direction. The electric conductivity in the fiber direction is set at $\sigma_x = 1.0$ S/m. The electrical conductivity in the thickness direction, the number of voltage measurement points (voltage electrode numbers), the crack depth and position are varied as shown in Table 1, which confirms that there is an effect on crack estimation accuracy. It should be noted that the electrodes placed on the specimen surface are assumed to be points having no width. Because practical applications of CFRP surfaces usually involve a coating with varnish or paint on the CFRP surface, it is recommended that the electrode be co-cured during CFRP processing [27] or that the surface undergo laser abrasion [33] to obtain good electric contacts between the CFRP and the electrodes. To produce multiple electrodes for practical applications, electrode pattern sheets fabricated by photolithography [34,35] and electroplating methods [36] were proposed.

A number (a maximum of 28) of 1-mm unit cracks were generated in a search region in the same layer as an estimated crack, at intervals of $x = -14$–14 mm. With CSI, a fixed doublet strength was calculated in the unit cracks, the true-value voltage distribution was calculated in a search region split into 0.2-mm intervals. A fixed doublet strength was calculated with high accuracy in the doublet intervals. An estimated crack is set at 7 mm in length. After the CSI search, if the cracks in the search area were below 2 mm,

Table 2
Parameters of GA for CSI.

Population	800
Max generation	1000
Mutation rate	0.2
Cross-over rate	0.8
Cross-over style	Two-point cross-over
Gene length	28
Selection style	Roulette selection

they were ignored because they were very small, and the estimation accuracy and error rate were calculated as described in the following section. The GA parameters used in this analysis are shown in Table 2.

3.2. Results and discussion

3.2.1. Effect of electric conductivity in the thickness direction on the accuracy of crack estimation

To improve the fracture toughness, in recent aircraft structures, interlaminar thermoplastic resins are sometimes added to composite laminates [37]. It is necessary to verify cases of low electric conductivity in the thickness direction. Here, estimation accuracy, *Acc* (overall accuracy), is defined as follows:

$$Acc = \frac{1}{N}\sum_{i=1}^{N_s} b_i \tag{18}$$

$$b_i = \begin{cases} 1 & \text{(if the estimation at interval } i \text{ matches)} \\ 0 & \text{(otherwise)} \end{cases} \tag{19}$$

As shown in Eq. (19), b_i is 1 if there is agreement between the presence or absence of a crack in the interval i of the search area and the true presence or absence of a crack; otherwise, its value is 0 (i.e., if there is no agreement). Therefore, *Acc* in Eq. (18) is the accuracy index, taking into account the location and size of the crack. In addition, commission errors are introduced, whereby unit cracks exist where true cracks do not exist, and omission errors are introduced, whereby unit cracks do not exist where true-value cracks do exist. Both of these errors are calculated.

Fig. 5(a) shows the resulting estimation accuracy if a crack of estimated length 7 mm occurs between $x = -12$–-5 mm. σ_z gradually decreases from an isotropic value of 0.01 S/m to the high anisotropic values of 0.008, 0.006, 0.004, 0.002, and 0.001 S/m. CSI is carried out ten times under the same conditions. As can be seen in the figure, until $\sigma_z = 0.004$ S/m, the estimation accuracy is shown to be high; however, after $\sigma_z = 0.002$ S/m, the omission error rate increases, and accurate crack estimations are no longer achieved. Fig. 5(b) shows the true voltage distribution if $\sigma_z = 0.01$ or 0.001 S/m. The reason for this phenomenon is thought to be that as the electric conductivity is lower, the electric current density in the thickness direction is lower in the crack location, and as it does not reach a local distribution, as in the case of $\sigma_z = 0.01$ S/m true value voltage distribution of Fig. 5(b), where there tend to be more errors. The computational time using the GA parameter in Table 1 is approximately 4.5 min using a PC (CPU: Core i7-2600, memory: 4.00 GB) for one calculation; it takes approximately 45 min for ten calculations.

3.2.2. Effect of the number of voltage measurement points on estimation accuracy

Based on real-world measurements, in practice, it is preferable to have fewer voltage electrodes. As shown in Table 3, estimation is carried out with five patterns of voltage measurement points. As shown in Fig. 6, the range of x and the interval in Table 3 indicate the distance between the outermost electrodes and the distance between adjacent electrodes, respectively. Fig. 7 shows the estimation accuracy that resulted from ten estimations of 7-mm cracks between $x = -12$–-5 mm. As can be seen in the figure, the crack

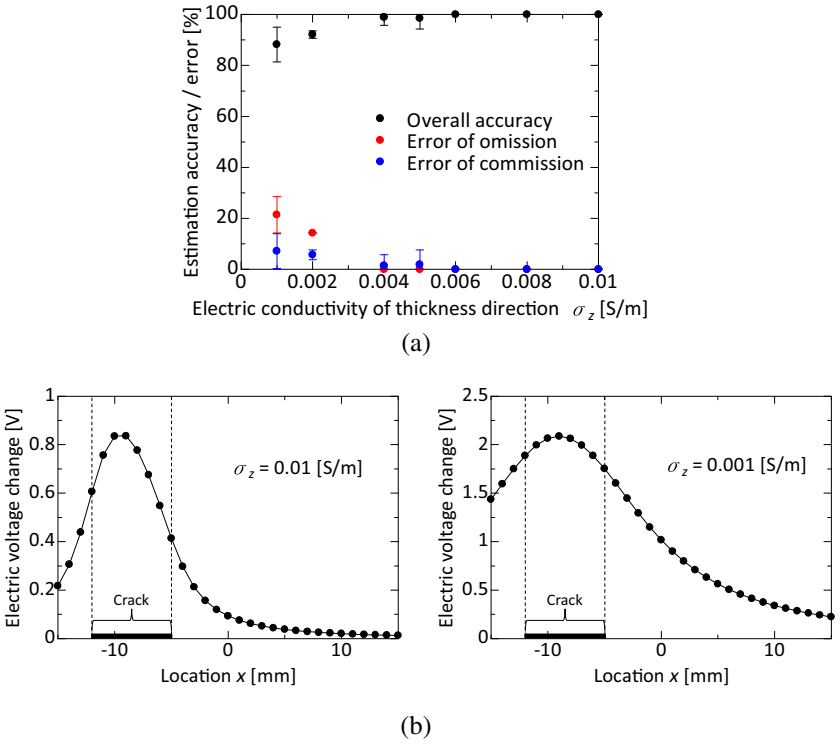

Fig. 5. Result of crack estimation in unidirectional laminate using CSI. Relationship of (a) electric conductivity in thickness direction to estimation accuracy and error and (b) location x and true electric voltage change on the specimen's surface. (Delamination crack $x = -12$–-5).

Table 3
Number of measurement points for CSI.

	Case1	Case2	Case3	Case4	Case5
Range of x	−15–15	−14–14	−15–15	−14–14	−10–10
Interval (mm)	1	2	5	7	10
Number of measurement points	31	15	7	5	3

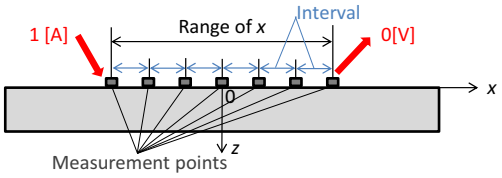

Fig. 6. Schematic of installed electrodes on the surface for CSI.

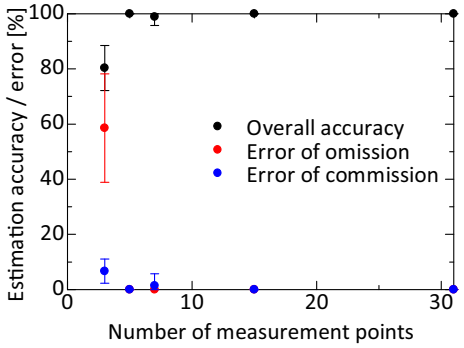

Fig. 7. Relationship of number of measurement points and estimation accuracy and error in unidirectional laminate using CSI. (Delamination crack $x = -12$–-5).

estimation accuracies are similar; the true values of cracks were estimated, except in the case of three voltage measurement points (Case 5). Based on this result, it is possible to detect cracks using electrode intervals smaller than the widths of the cracks to be detected.

3.2.3. Effect of crack depth on estimation accuracy

Fig. 8(a) shows an estimation accuracy distribution map that calculates the estimation accuracy while changing the location of the 7-mm wide cracks at 2-mm intervals for each layer. Representative center points of the 7-mm cracks are plotted. Ten crack estimations were carried out under the same conditions. Additionally, Fig. 8(b) shows the absolute value of the electric current density in the thickness direction at each crack location.

As can be seen in Fig. 8(a), 7-mm-wide cracks were generally detected with over 80% accuracy across the laminated plate. Furthermore, Fig. 8(a) and (b) show that the estimation accuracy is higher near a current electrode where the electric current density in the thickness direction is high. The closer the estimated crack is to the center of a current electrode or the deeper the layer, the lower the estimation accuracy. Fig. 9 shows the relationship between the omission error rate and the electric current density in the thickness direction at the corresponding position. We observe that the lower the electric current density in the thickness direction, the greater the omission error rate. To ensure a high estimation accuracy, the electric current in the thickness direction must have a high value, which is obtained by adjusting the electrode interval considering anisotropic electric conductivity.

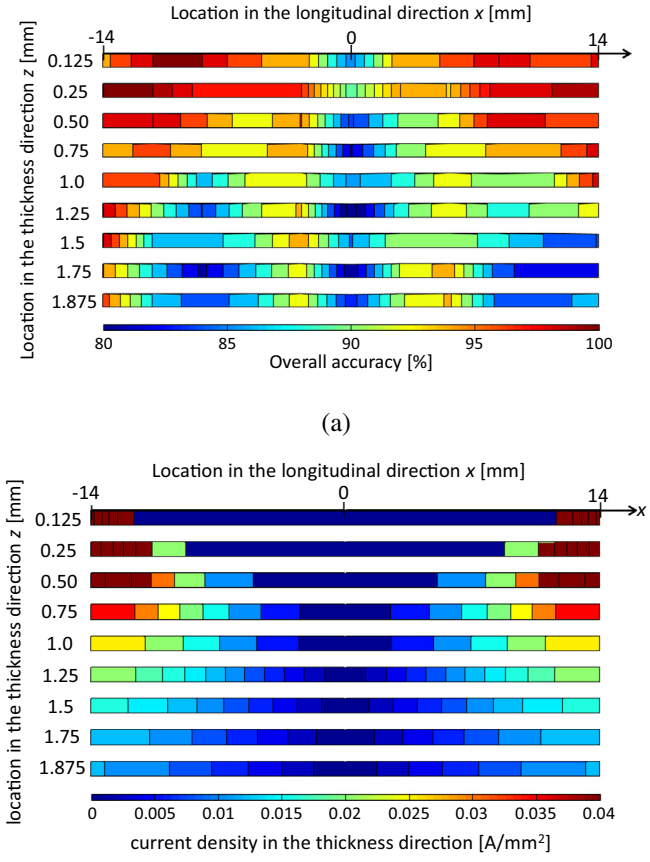

Fig. 8. Result of crack estimation in unidirectional laminate using CSI. Relationship of (a) overall accuracy of crack estimation to depth of the crack and (b) current density in the thickness direction to depth of the crack.

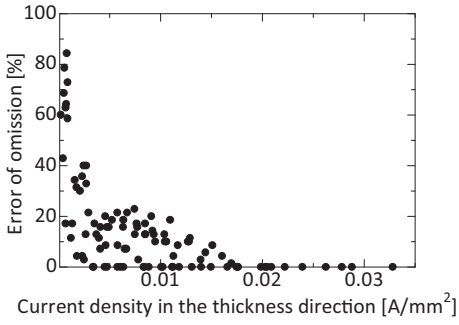

Fig. 9. Relationship of current density in the thickness direction to error of omission in unidirectional laminate using CSI.

4. Conclusions

This paper proposed crack swarm inspection, with the goal of estimating crack locations and sizes from the surface voltage

distribution of a cracked composite material by introducing a genetic algorithm for crack analysis with doublets. By applying the technique to cracked CFRP laminated plates, the estimation accuracy was validated for the electric conductivity, voltage measurement points, and crack depth. The lower the electric conductivity in the thickness direction, the more difficult crack detection becomes, because the voltage change distribution caused by crack development does not have sharp peaks in regions close to the crack. It is possible to detect cracks with voltage measurement points by installing electrodes at smaller intervals than the width of the cracks to be detected. Furthermore, it was confirmed that 7-mm cracks were detected with a degree of accuracy of over 80%. It was also confirmed that the electric current density in the thickness direction around the crack location affects the estimation accuracy. By calculating the equivalent electric conductivity, the proposed method can be extended to multidirectional laminates. Because the accuracy of the estimation depends on the electric conductivity ratio (σ_z/σ_x), this method would be more accurate in multidirectional laminates, which have smaller σ_x compared with unidirectional laminates.

References

[1] Harris CE, Starnes JH, Shuart MJ. Design and manufacturing of aerospace composite structures, state-of-the-art assessment. J Aircr 2002;39(4):545–60.
[2] Gate D. Boeing 787 wing flaw extends inside plane. Seattle Times; 2009.
[3] Sanchez-Saez S, Barbero E, Zaera R, Navarro C. Compression after impact of thin composite laminates. Compos Sci Technol 2005;65(13):1911–9.
[4] Freemantle RJ, Hankinson N, Brotherhood CJ. Rapid phased array ultrasonic imaging of large area composite aerospace structures. Insight-Non-Destr Test Condition Monit 2005;47:129–32.
[5] Staszewski WJ, Mahzan S, Traynor R. Health monitoring of aerospace composite structures – active and passive approach. Compos Sci Technol 2009;69(11–12):1678–85.
[6] Katunin A, Dragan K, Dziendzikowski M. Damage identification in aircraft composite structures: a case study using various non-destructive testing techniques. Compos Struct 2015;127:1–9.
[7] Schilling PJ, Karedla BR, Tatiparthi AK, Verges MA, Herrington PD. X-ray computed microtomography of internal damage in fiber reinforced polymer matrix composites. Compos Sci Technol 2005;65(14):2071–8.
[8] Jasiūnienė E, Raišutis R, Šliteris R, Voleišis A, Vladišauskas A, Mitchard D, et al. NDT of wind turbine blades using adapted ultrasonic and radiographic techniques. Insight 2009;51(9):477–83.
[9] Dutta D, Sohn H, Harries KA, Rizzo P. A nonlinear acoustic technique for crack detection in metallic structures. Struct Health Monit 2009;8(3):251–62.
[10] Boominathan R, Arumugam V, Santulli C, Adhithya Plato Sidharth A, Anand Sankar R, Sridhar BTN. Acoustic emission characterization of the temperature effect on falling weight impact damage in carbon/epoxy laminates. Compos B Eng 2014;56:591–8.
[11] Takeda S, Okabe Y, Takeda N. Delamination detection in CFRP laminates with embedded small-diameter fiber Bragg grating sensors. Compos A Appl Sci Manuf 2002;33(7):971–80.
[12] Okabe Y, Tsuji R, Takeda N. Application of chirped fiber Bragg grating sensors for identification of crack locations in composites. Compos A Appl Sci Manuf 2004;35(1):59–65.
[13] Antunes P, Varum H, Andréa P. Optical FBG sensors for static structural health monitoring. Proc Eng 2011;14:1564–71.
[14] Owston CN. Electrical properties of single carbon fibres. J Phys D Appl Phys 1970;3(11):1615–26.
[15] Wang X, Chung DDL. Piezoresistive behavior of carbon fiber in epoxy. Carbon 1997;35:1649–79.
[16] Kupke M, Schulte K, Schüler R. Non-destructive testing of FRP by d.c. and a.c. electrical methods. Compos Sci Technol 2001;61(6):837–47.
[17] Prasse T, Michel F, Mook G, Schulte K, Bauhofer W. A comparative investigation of electrical resistance and acoustic emission during cyclic loading of CFRP laminates. Compos Sci Technol 2001;61(6):831–5.
[18] Angelidis N, Wei CY, Irving PE. The electrical resistance response of continuous carbon fibre composite laminates to mechanical strain. Compos A Appl Sci Manuf 2004;35(10):1135–47.
[19] Weber I, Schwartz P. Monitoring bending fatigue in carbon-fibre/epoxy composite strands: a comparison between mechanical and resistance techniques. Compos Sci Technol 2001;61(6):849–53.
[20] Gadomski J, Pyrzanowski P. Damage identification in strongly loaded carbon-reinforced composite using the electric resistance change procedure. Mater Test 2011;53(6):351–5.
[21] Pyrzanowski P, Olzak M. Numerical modelling of resistance changes in symmetric CFRP composite under the influence of structure damage. Compos Sci Technol 2013;88:99–105.
[22] Seo D-C, Lee J-J. Damage detection of CFRP laminates using electrical resistance measurement and neural network. Compos Struct 1999;47(1–4):525–30.
[23] Sevkat E, Li J, Liaw B, Delale F. A statistical model of electrical resistance of carbon fiber reinforced composites under tensile loading. Compos Sci Technol 2008;68(10–11):2214–9.
[24] Tada N, Hayashi Y, Kitamura T, Ohtani R. Analysis on the applicability of direct current electrical potential method to the detection of damage by multiple small internal cracks. Int J Fract 1997;85(1):1–9.
[25] Akama M, Saka M. Nondestructive sizing of a 3D surface crack generated in a railway component using closely coupled probes for direct-current potential drop technique. Eng Fract Mech 2005;72(2):319–34.
[26] Ueda M, Todoroki A. Asymmetrical dual charge EPCM for delamination monitoring of CFRP laminate. Key Eng Mater 2006;321–323:1309–15.
[27] Ueda M, Todoroki A. Delamination monitoring of CFRP laminate using the two-stage electric potential change method with equivalent electric conductivity. Eng Fract Mech 2008;75(9):2737–50.
[28] Todoroki A. Electric current analysis of CFRP using perfect fluid potential flow. Trans Jpn Soc Aeronaut Space Sci 2012;55(3):183–90.
[29] Todoroki A, Arai M. Simple electric-voltage-change analysis method for delamination of thin CFRP laminates using anisotropic electric potential function. Adv Compos Mater 2014;23(3):261–73.
[30] Joseph Katz AP. Low-speed aerodynamics. Cambridge University Press; 2001.
[31] Özisik MN. Heat conduction. 2nd ed. John Wiley & Sons Inc; 1993.
[32] Melanie M. An introduction to genetic algorithms. A bradford book; 1998.
[33] Fischer F, Kreling S, Jäschke P, Frauenhofer M, Kracht D, Dilger K. Laser surface pre-treatment of CFRP for adhesive bonding in consideration of the absorption behaviour. J Adhes 2012;88(4–6):350–63.
[34] Kobayashi S, Matsuzaki R, Todoroki A. Multipoint cure monitoring of CFRP laminates using a flexible matrix sensor. Compos Sci Technol 2009;69(3–4):378–84.
[35] Matsuzaki R, Kobayashi S, Todoroki A, Mizutani Y. Full-field monitoring of resin flow using an area-sensor array in a VaRTM process. Compos A Appl Sci Manuf 2011;42(5):550–9.
[36] Todoroki A, Samejima Y, Hirano Y, Matsuzaki R, Mizutani Y. Mechanism of electrical resistance change of a thin CFRP beam after delamination cracking. J Solid Mech Mater Eng 2010;4(1):1–11.
[37] Wang P, Hamila N, Boisse P, Chaudet P, Lesueur D. Thermo-mechanical behavior of stretch-broken carbon fiber and thermoplastic resin composites during manufacturing. Polym Compos 2015;36(4):694–703.